

# Interfacial Nanochemistry

# Nanostructure Science and Technology

Series Editor: David J. Lockwood, FRSC  
*National Research Council of Canada  
Ottawa, Ontario, Canada*

---

*Current volumes in this series:*

Alternative Lithography: Unleashing the Potentials of Nanotechnology  
*Edited by Clivia M. Sotomayor Torres*

Interfacial Nanochemistry: Molecular Science and Engineering at Liquid-Liquid Interfaces  
*Edited by Hitoshi Watarai*

Nanoparticles: Building Blocks for Nanotechnology  
*Edited by Vincent Rotello*

Nanostructured Catalysts  
*Edited by Susannah L. Scott, Cathleen M. Crudden, and Christopher W. Jones*

Nanotechnology in Catalysis, Volumes 1 and 2  
*Edited by Bing Zhou, Sophie Hermans, and Gabor A. Somorjai*

Polyoxometalate Chemistry for Nano-Composite Design  
*Edited by Toshihiro Yamase and Michael T. Pope*

Self-Assembled Nanostructures  
*Jin Z. Zhang, Zhong-lin Wang, Jun Liu, Shaowei Chen, and Gang-yu Liu*

Semiconductor Nanocrystals: From Basic Principles to Applications  
*Edited by Alexander L. Efros, David J. Lockwood, and Leonid Tsybeskov*

---

# Interfacial Nanochemistry

## Molecular Science and Engineering at Liquid–Liquid Interfaces

Edited by

**Hitoshi Watarai**

*Osaka University  
Osaka, Japan*

**Norio Teramae**

*Tohoku University  
Tohoku, Japan*

and

**Tsuguo Sawada**

*Tokyo University  
Tokyo, Japan*

**Kluwer Academic / Plenum Publishers**

New York, Boston, Dordrecht, London, Moscow

Library of Congress Cataloging-in-Publication Data

---

Watarai, Hitoshi.

Interfacial nanochemistry : molecular science and engineering at liquid-liquid interfaces /  
Professor Hitoshi Watarai.

p. cm.—(Nanostructure science and technology)

Includes bibliographical references and index.

ISBN 0-306-48527-3

I. Liquid-liquid interfaces. I. Title. II. Series.

QD509.L54W37 2005

541'.33—dc22

2004055312

---

ISBN 0-306-48527-3

© 2005 Kluwer Academic/Plenum Publishers, New York  
233 Spring Street, New York, New York 10013

<http://www.kluweronline.com>

10 9 8 7 6 5 4 3 2 1

A C.I.P. record for this book is available from the Library of Congress

All rights reserved

No part of this work may be reproduced, stored in a retrieval system, or transmitted in any form or by any means, electronic, mechanical, photocopying, microfilming, recording, or otherwise, without written permission from the Publisher, with the exception of any material supplied specifically for the purpose of being entered and executed on a computer system, for exclusive use by the purchaser of the work

Permissions for books published in Europe: [permissions@wkap.nl](mailto:permissions@wkap.nl)

Permissions for books published in the United States of America: [permissions@wkap.com](mailto:permissions@wkap.com)

Printed in the United States of America.

# Contributors

**Raymond R. Dagastine**  
Department of Chemical and  
Biomolecular Engineering  
University of Melbourne  
Melbourne, Victoria 3010  
Australia

**Jeremy G. Frey**  
Department of Chemistry  
University of Southampton  
Southampton SO17 1BJ  
UK

**Masahiro Goto**  
Department of Applied Chemistry  
Graduate School of Engineering  
Kyushu University  
Fukuoka 812-8581  
Japan

**Fumio Hirata**  
Institute for Molecular Science  
Okazaki National Research Institutes  
Myodaiji, Okazaki 444-8585  
Japan

**Hiroki Hotta**  
Department of Chemistry  
Kobe University  
Nada, Kobe 657-8501  
Japan

**Yasuhiro Ikezoe**  
Department of Advanced Materials  
Science  
Graduate School of Frontier  
Sciences  
The University of Tokyo  
Hongo, Tokyo 113-8656  
Japan

**Shoji Ishizaka**  
Department of Chemistry  
Graduate School of Science  
Hokkaido University  
Sapporo 060-0810  
Japan

**Takashi Kakiuchi**  
Department of Energy and  
Hydrocarbon Chemistry  
Graduate School of Engineering  
Kyoto University  
Kyoto 606-8501  
Japan

**Sorin Kihara**  
Department of Chemistry  
Kyoto Institute of Technology  
Matsugasaki  
Sakyo, Kyoto 606-8585  
Japan

**Noboru Kitamura**  
Department of Chemistry  
Graduate School of Science  
Hokkaido University  
Sapporo 060-0810  
Japan

**Shū Kobayashi**  
Graduate School of Pharmaceutical  
Sciences  
The University of Tokyo  
Hongo  
Bunkyo-ku, Tokyo 113-0033  
Japan

**Andriy Kovalenko**  
National Institute for Nanotechnology  
National Research Council of Canada  
University of Alberta  
9107-116 Str.  
Edmonton, AB T6G 2V4  
Canada

**Kei Manabe**  
Graduate School of Pharmaceutical  
Sciences  
The University of Tokyo  
Hongo  
Bunkyo-ku, Tokyo 113-0033  
Japan

**Kiyoharu Nakatani**  
Department of Chemistry  
University of Tsukuba  
Tennoudai, Tsukuba 305-8571  
Japan

**Takayuki Negishi**  
Department of Chemistry  
University of Tsukuba  
Tennoudai, Tsukuba 305-8571  
Japan

**Seiichi Nishizawa**  
Department of Chemistry  
Graduate School of Science

Tohoku University  
Aoba-ku, Sendai 980-8578  
Japan

**Tsutomu Ono**  
Department of Applied Chemistry  
Graduate School of Engineering  
Kyushu University  
Fukuoka 812-8581  
Japan

**Toshiyuki Osakai**  
Department of Chemistry  
Kobe University  
Nada, Kobe 657-8501  
Japan

**Geraldine L. Richmond**  
Department of Chemistry  
and Materials Science Institute  
University of Oregon  
Eugene, OR 97403  
USA

**Tsuguo Sawada**  
Department of Advanced Materials  
Science  
Graduate School of Frontier Sciences  
The University of Tokyo  
Hongo, Tokyo 113-8656  
Japan

**Geoffery W. Stevens**  
Department of Chemical and  
Biomolecular Engineering  
University of Melbourne  
Melbourne, Victoria 3010  
Australia

**Norio Teramae**  
Department of Chemistry  
Graduate School of Science  
Tohoku University  
Aoba-ku, Sendai 980-8578  
Japan

**Satoshi Tsukahara**

Department of Chemistry  
Graduate School of Science  
Osaka University  
Toyonaka, Osaka 560-0043  
Japan

**Tatsuya Uchida**

Tokyo University of Pharmacy and  
Life Science  
Hachioji 192-0392  
Japan

**Hitoshi Watarai**

Department of Chemistry  
Graduate School of Science  
Osaka University  
Toyonaka, Osaka 560-0043  
Japan

**Mark R. Watry**

Rocky Mountain College  
Billings, MT 59102  
USA

**Akira Yamaguchi**

Department of Chemistry  
Graduate School of Science  
Tohoku University  
Aoba-ku, Sendai 980-8578  
Japan

**Hiroharu Yui**

Department of Advanced Materials  
Science  
Graduate School of Frontier  
Sciences  
The University of Tokyo  
Hongo, Tokyo 113-8656  
Japan

# Preface

The history of the liquid–liquid interface on the earth might be as old as that of the liquid. It is plausible that the generation of the primitive cell membrane is responsible for an accidental advent of the oldest liquid interfaces, since various compounds can be concentrated by an adsorption at the interface. The presence of liquid–liquid interface means that real liquids are far from ideal liquids that must be miscible with any kinds of liquids and have no interface. Thus it can be said that the non-ideality of liquids might generate the liquid–liquid interface indeed and that biological systems might be generated from the non-ideal interface. The liquid–liquid interface has been, therefore, studied as a model of biological membrane.

From pairing two-phases of gas, liquid and solid, nine different pairs can be obtained, which include three homo-pairs of gas–gas, liquid–liquid and solid–solid pairs. The gas–gas interface, however, is practically no use under the ordinary conditions. Among the interfaces produced by the pairing, the liquid–liquid interface is most slippery and difficult to be studied experimentally in comparison with the gas–liquid and solid–liquid interfaces, as the liquid–liquid interface is flexible, thin and buried between bulk liquid phases. Therefore, in order to study the liquid–liquid interface, the invention of innovative measurement methods has a primary importance.

At the liquid–liquid interface, completely different properties of water and organic phases can be met in the two-dimensional boundary with a thickness of only 1 nm. In practical two-phase systems with highly miscible components, however, the formation of nano- and micro-droplets at the interfacial nano-region is suggested. The structural and dynamic properties of molecules at the interface are the most important subject in the study of physics and chemistry at the interface. The solution theory of the liquid–liquid interface has not been established yet, though the molecular dynamics simulations have been developed as a useful tool for depicting the molecular picture of the solvent and solute molecules in the interfacial region.

The adsorption of reactant molecules at the interface significantly affects the overall reaction rate in the two-phase system by the catalytic function of the interface. The liquid–liquid interface itself is a unique catalyst with such a flexible adsorbed area, which can be expanded or shrunk easily only by stirring or shaking. The increase of the adsorbed reactant molecules results in the promotion of reaction rate and the product will be extracted into the organic phase depending on its hydrophobicity.

The accumulation of solute molecule at the interface is ready to produce assemblies or aggregates at the interface with somewhat oriented structure. Molecular network and two-dimensionally stacked compound can be produced at the interface. These aggregates exhibit molecular recognizing ability very often. Studies of these functions are very important to understand the role of biological membrane and protein–interface interaction at the membrane.

This book is intended to make clear the front of the state-of-the art of the nanochemistry of the liquid–liquid interface. The plan to make this book had started from the discussion with Mr. Kenneth Howell of Kluwer Academic Publishers just after the Symposium on “Nano-Chemistry in Liquid–Liquid Interfaces” at the Pacificchem 2001 held in Hawaii. In the year of 2001, the Scientific Research on Priority Areas “Nano-Chemistry at the Liquid–Liquid Interfaces” (2001–2003) was approved by the Ministry of Education, Culture, Sports, Science and Technology of Japan. So, it will be timely to review some important studies accomplished in the project and to learn more about the liquid–liquid interfacial science by inviting outstanding researchers through the world as authors.

The title of this book is Interfacial Nanochemistry, but almost all the chapters are devoted to the research of the liquid–liquid interface and the unique chemistry at the interface. In spite of its being the most important interface for our biological world, we have the least knowledge about it. It might be our great pleasure if our readers could find any new concepts on the physical and chemical functions of the liquid–liquid interface in this book. I sincerely wish readers to improve their knowledge on the liquid–liquid interface and to produce any new ideas for the research or application of the liquid–liquid interface.

I would like to express my sincere thanks to the authors for submitting their worthy accomplishment and to the members of the Scientific Research of Priority Areas “Nano-Chemistry at the Liquid–Liquid Interfaces” for cooperating to build the new field of Interfacial Nanochemistry. I am deeply indebted to Dr. Hideo Akaiwa, a president of Gunma University, and Professor Fumiyuki Nakashio of Sojyo University for the success in our project. I also thank Mr. Kenneth Howell for his kind encouragement to produce this book, and Ms. Keiko Kaihatsu for her efforts on editing the manuscripts. This work was in part supported by the Ministry of Education, Culture, Sports, Science and Technology of Japan.

Hitoshi Watarai  
Osaka, Japan

# Contents

<b>CHAPTER 1. Second Harmonic Generation at Liquid/Liquid Interfaces.....</b>	<b>1</b>
<i>Jeremy G. Frey</i>	
1.1 Introduction .....	1
1.2 SHG theory .....	2
1.3 Experimental techniques .....	6
1.4 The bare hydrocarbon/water interface .....	7
1.5 Adsorption of <i>para</i> -nitrophenol .....	7
1.6 Flow cell experiments .....	10
1.7 Dye molecules at the dodecane/water interface .....	13
1.8 Electrochemical liquid/liquid interfaces .....	15
1.9 Chiral molecules at liquid/liquid interfaces .....	16
1.10 SHG from micelles and liposomes .....	17
1.11 Concluding remarks .....	19
<b>CHAPTER 2. Vibrational Sum-Frequency Spectroscopic Investigations of Molecular Interactions at Liquid/Liquid Interfaces.....</b>	<b>25</b>
<i>Mark R. Watry and Geraldine L. Richmond</i>	
2.1 Introduction .....	25
2.2 Theoretical considerations of VSFS .....	26
2.3 Experimental considerations .....	36
2.4 Applications .....	37
2.5 Summary and future directions .....	56
<b>CHAPTER 3. Observation of Dynamic Molecular Behaviour at Liquid/Liquid Interfaces by Using the Time-Resolved Quasi-Elastic Laser Scattering Method.....</b>	<b>59</b>
<i>Hiroharu Yui, Yasuhiro Ikezoe and Tsuguo Sawada</i>	
3.1 Introduction .....	59
3.2 Time-resolved quasi-elastic laser scattering method .....	60
3.3 A phase transfer catalytic reaction at a liquid/liquid interface .....	64

3.4	A chemical oscillation induced by anionic surfactant at a w/nb interface .....	69
3.5	Concluding remarks .....	74
<b>CHAPTER 4. Direct Force Measurement at Liquid/Liquid Interfaces.....</b>		<b>77</b>
<i>Raymond R. Dagastine and Geoffery W. Stevens</i>		
4.1	Introduction .....	77
4.2	Types of colloidal forces .....	79
4.3	Atomic force microscopy at rigid interfaces .....	82
4.4	Force measurements at liquid interfaces .....	84
4.5	General behaviour of forces at liquid interfaces .....	89
4.6	Concluding remarks .....	92
<b>CHAPTER 5. A Molecular Theory of Solutions at Liquid Interfaces.....</b>		<b>97</b>
<i>Andriy Kovalenko and Fumio Hirata</i>		
5.1	Introduction .....	97
5.2	Molecular theory of fluid phase equilibria .....	100
5.3	Microscopic description of liquid/liquid and liquid/vapour interfaces .....	103
<b>CHAPTER 6. Electrochemical Processes at Aqueous/Organic Solution or Aqueous/Membrane Interfaces.....</b>		<b>127</b>
<i>Sorin Kihara</i>		
6.1	Introduction .....	127
6.2	Voltammogram for ion transfer at the w/o interface .....	128
6.3	Voltammogram for electron transfer at the w/o interface .....	131
6.4	Ion transfer coupled with electron transfer at the w/o interface .....	132
6.5	Process of ion transport through a membrane .....	138
6.6	New types of membrane reactions mimicking biological processes [27,28] .....	141
6.7	Oscillation of membrane current or membrane potential [32] .....	145
6.8	Conclusion .....	152
<b>CHAPTER 7. Electrochemical Instability at Liquid/Liquid Interfaces.....</b>		<b>155</b>
<i>Takashi Kakiuchi</i>		
7.1	Introduction .....	155
7.2	Theoretical background .....	156
7.3	Experimental features of electrochemical instability in electrochemical transfer of ionic surfactant across the liquid/liquid interface .....	165
7.4	Conclusions .....	168

<b>CHAPTER 8. Electron Transfer at Liquid/Liquid Interfaces</b> .....	<b>171</b>
<i>Toshiyuki Osakai and Hiroki Hotta</i>	
8.1 Introduction .....	171
8.2 Electron transfer at the polarizable o/w interface .....	172
8.3 New methodologies .....	175
8.4 Reaction mechanisms .....	177
8.5 Concluding remarks .....	185
<b>CHAPTER 9. Mass Transfer and Reaction Rate in the Nano-Region of Microdroplet/Solution Interfaces</b> .....	<b>189</b>
<i>Kiyoharu Nakatani and Takayuki Negishi</i>	
9.1 Introduction .....	189
9.2 Manipulation, electrochemistry and spectroscopy of single microdroplets .....	190
9.3 Microdroplet size effect on mass transfer and reaction rate .....	192
9.4 Simple ion-pair extraction in a single micro-oil-droplet/water system .....	194
9.5 Ion-pair extraction of an anionic surfactant with a cationic dye .....	198
9.6 Concluding remarks .....	203
<b>CHAPTER 10. Single Molecule Diffusion and Metal Complex Formation at Liquid/Liquid Interfaces</b> .....	<b>205</b>
<i>Hitoshi Watarai and Satoshi Tsukahara</i>	
10.1 Introduction .....	205
10.2 Interfacial diffusion dynamics .....	207
10.3 Interfacial catalysis .....	214
10.4 Interfacial aggregation .....	223
10.5 Concluding remarks .....	228
<b>CHAPTER 11. Molecular Recognition of Ions at Liquid/Liquid Interfaces</b> .....	<b>233</b>
<i>Norio Teramae, Seiichi Nishizawa, Akira Yamaguchi, and Tatsuya Uchida</i>	
11.1 Introduction .....	233
11.2 Hydrogen-bond-mediated anion recognition at L/L interfaces .....	234
11.3 Molecular recognition at L/L interfaces as studied by second harmonic generation spectroscopy .....	239
11.4 Concluding remarks .....	246
<b>CHAPTER 12. Photochemistry at Liquid/Liquid Interfaces</b> .....	<b>249</b>
<i>Shoji Ishizaka and Noboru Kitamura</i>	
12.1 Introduction .....	249
12.2 Theoretical and experimental backgrounds .....	250
12.3 TIR fluorescence dynamic anisotropy at a liquid/liquid interface .....	253

12.4	Excitation energy transfer and its dynamics at a water/oil interface .....	257
12.5	Structures at a liquid/liquid interface .....	259
12.6	A relationship between interfacial structure and polarity at a liquid/liquid interface .....	264
12.7	Photochemical observation of molecular recognition at a liquid/liquid interface .....	266
12.8	Concluding remarks .....	267
<b>CHAPTER 13. Development of Surfactant-Type Catalysts for Organic Synthesis in Water .....</b>		<b>271</b>
<i>Kei Manabe and Shū Kobayashi</i>		
13.1	Introduction .....	271
13.2	Surfactant-type Lewis acids for reactions in water .....	273
13.3	Surfactant-type Brønsted acids for reactions in water .....	278
13.4	Concluding remarks .....	284
<b>CHAPTER 14. Bioseparation Through Liquid–Liquid Interfaces.....</b>		<b>287</b>
<i>Tsutomu Ono and Masahiro Goto</i>		
14.1	Introduction .....	287
14.2	Reverse micellar protein extraction .....	287
14.3	Extraction of DNA through liquid–liquid interfaces .....	298
14.4	Concluding remarks .....	302
<i>Index</i> .....		303

# 1

## Second Harmonic Generation at Liquid/Liquid Interfaces

Jeremy G. Frey

*School of Chemistry, University of Southampton, Southampton, UK*

### 1.1. INTRODUCTION

Processes occurring at the interface between two immiscible liquids underlie many important phenomena in chemistry and biology, including liquid extraction, liquid chromatography, phase transfer catalysis, membrane processes and drug delivery. Understanding the role of structure and dynamics of these interfaces on adsorption to, solvation at and transfer across the interface is of direct relevance to these physicochemical processes. The study of such interfaces by macroscopic measurements such as surface tension while yielding significant information on the interfacial properties cannot yield microscopic or molecular detail. The non-linear optical techniques of second harmonic generation (SHG) and sum frequency generation (SFG) have been useful in probing the liquid/liquid interface.

SHG is a coherent process and in principle the experimental system needed to observe the response is very simple. The fundamental radiation from a laser source incident at an interface generates the harmonic beam via non-linear polarization of the medium. Typically, this beam is observed in reflection, but many studies have been undertaken in total internal reflection and transmission geometries. As the harmonic beam is well separated from the fundamental in frequency, it can be detected; the difficulties arise due to the inherent inefficiency of the harmonic generation and the low intensities that need to be detected. The sensitivity and selectivity of SHG to the interfacial species in the presence of the same species in the bulk phase provides the driving force to overcome these experimental difficulties.

There are several reviews of interfacial SHG which cover the theory and applications of SHG in general and describe some applications to the liquid/liquid interface [1–5]. In particular, the chapter by Brevet and Girault on Second Harmonic Generation at

Liquid/Liquid Interfaces [6] is an excellent discussion of the topic. In this review I will focus on a number of different examples of the application of SHG to liquid/liquid studies mainly from my own research group.

## 1.2. SHG THEORY

The SHG signals arise from the second-order polarization  $\mathbf{P}^{(2)}$  induced in a non-centrosymmetric medium by the electric field  $\mathbf{E}(\omega)$  of the incident fundamental radiation given by the tensor equation

$$\mathbf{P}^{(2)}(\omega) = \varepsilon_0 \chi^{(2)} \mathbf{E}(\omega) \mathbf{E}(\omega) \quad (1)$$

where  $\chi_{ijk}^{(2)}$  is the third rank tensor expressing the second-order surface susceptibility of the material. In a centrosymmetric medium, no second-order polarization is possible in the dipole approximation. At an interface, the inversion symmetry is broken and a dipole contribution to  $\mathbf{P}^{(2)}$  is allowed. The polarization at the interface is usually treated as a sheet of thickness much smaller than the wavelength of light. This polarized sheet gives rise to the harmonic wave generated in reflection or transmission, with the propagation directions being defined by conservation of momentum.

Equation (1) does hide some of the complexities as it emphasizes the local response, but the non-local terms can be significant and, for example, higher order quadropolar terms and terms involving the electric field gradient or magnetic terms lead to contributions to the SHG signal from the bulk. These terms all involve a derivative of the electric field vector. For most materials the magnetic terms are not significant and the electric quadrupole term provides the main contribution from the bulk. If SHG studies are extended to ferroelectric fluids, the magnetic term may need to be included.

The intensity  $I(2\omega)$  of the SHG signal observed from an interface between two isotropic bulk phases illuminated with fundamental radiation of intensity  $I(\omega)$  is given by [7]

$$I(2\omega) = \frac{32\pi^3 \omega^2}{c^2} \frac{\sqrt{\varepsilon_1(2\omega)}}{\varepsilon_1(\omega) (\varepsilon(2\omega) - \varepsilon_1(2\omega) \sin^2 \theta_1(2\omega))} |\mathbf{e}(2\omega) \cdot \chi^{(2)} \cdot \mathbf{e}(\omega) \mathbf{e}(\omega)|^2 I^2(\omega) \quad (2)$$

where  $\mathbf{e}(\omega)$  and  $\mathbf{e}(2\omega)$  are the polarization vectors for the fundamental and harmonic beams and include the appropriate combination of Fresnel factors. The refractive indices and permittivities  $\varepsilon_i$ , are defined for each layer of the three-layer model (Figure 1.1) and  $\theta_1$  is the angle of reflection of the harmonic beam in the upper layer. As written, Equation (2) applies when the permittivities are real and a more general expression is given by Brevet [7]. As explained by Brevet (chapter 7), for the three-layer model it is the real parts of the permittivity that are significant for the leading terms in Equation (2), though the full complex quantities are involved in the calculation of the Fresnel factors.

For an isotropic (in-plane) interface, only four of the tensor components,  $\chi_{ZZZ}$ ,  $\chi_{ZZX}$ ,  $\chi_{XZX}$  and  $\chi_{XYZ}$  where  $Z$  is the normal to the interface, contribute to the observed harmonic signal. The electric field of the S( $E_{2\omega}^S$ ) and P( $E_{2\omega}^P$ ) polarized components of the harmonic beam as a function of the linear polarization angle ( $\gamma$ ) of the fundamental

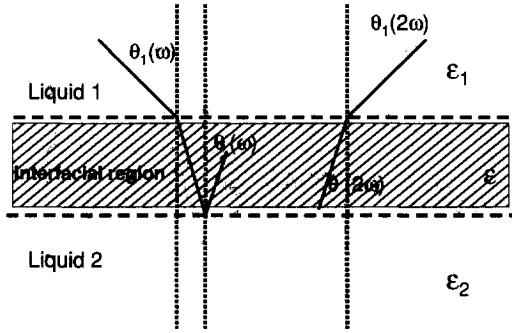


FIGURE 1.1. Layer model with the permittivity associated with each layer. The upper bulk phase is region 1 and the lower bulk phase surrounding the interface is region 2. The interface is considered as a microscopically thin region between the two bulk phases. In general, for a liquid/liquid or liquid/solid interface, dispersion may be significant and the reflection angle for the harmonic will differ slightly from the angle of incidence of the fundamental.

wave (assuming a pure linear polarization) are given by

$$E_{2\omega}^S = S (a_1 \chi_{XZX} \sin 2\gamma + a_6 \chi_{XYZ} \cos^2 \gamma) \quad (3)$$

$$E_{2\omega}^P = S \left( (a_2 \chi_{XZX} + a_3 \chi_{ZXX} + a_4 \chi_{ZZZ}) \cos^2 \gamma + a_5 \chi_{ZXX} \sin^2 \gamma - a_7 \chi_{XYZ} \sin 2\gamma \right) \quad (4)$$

The  $\chi_{XYZ}$  component is only non-zero for chiral surfaces; the value of  $\chi_{XYZ}$  for two enantiomers will be equal in magnitude but opposite in sign. As the tensor components can be complex quantities (especially near resonance), the harmonic wave can be elliptically polarized even for a linearly polarized fundamental, just as in conventional ellipsometry. This results in a variety of interesting effects of non-linear optical activity being observable in SHG [8–13]. The majority of observations of this type have been made on chiral films [14,15].

The  $a_i$  coefficients are combinations of Fresnel factors relating the electric fields in the interfacial region to the external field and they depend on the exact model for the interface chosen. For the second harmonic calculations, a simple three-layer model (Figure 1.1) is typically used. The non-linear region is the thin layer between bulk immersion medium layers. It is important to realize that this layer is assumed always to be vanishing thin, being on the order of the molecular dimension of the target, because thicker assemblies of molecules are usually centrosymmetric and do not generate even harmonics. The second harmonic calculations therefore assume that there is no significant light interference in this layer, although there is reflection at its upper and lower boundaries. This is in contrast to macroscopic layered structures often investigated by linear ellipsometry, where interference effects within the layer can contribute dominantly to the overall polarization changes.

In the absence of chiral effects it is often convenient to fit the polarization data, in the first instance, to the phenomenological equations (5) and (6) that describe the expected shape of the polarization behaviour [16]. For the P-polarized harmonic intensity,  $I_P$  is

given by

$$I_P = |A \cos^2 \gamma + B \sin^2 \gamma|^2 \quad (5)$$

and for the S-polarized harmonic intensity,  $I_S$  is given by

$$I_S = |C \sin 2\gamma|^2 \quad (6)$$

where  $\gamma = 0^\circ$  corresponds to P-polarized and  $\gamma = 90^\circ$  to S-polarized fundamental fields. The parameters  $A$ ,  $B$  and  $C$ , which may be complex, are linear combinations of the components of the second-order susceptibility,  $\chi$  tensor, and the non-linear Fresnel coefficients,  $a_i$ . This allows the initial model to be fit without the concern of the often unknown interfacial refractive index that is required to evaluate the Fresnel coefficients,  $a_i$ . More details of this procedure and the model-dependent assumptions used in the data analysis are discussed later.

The additional terms that need to account for the main non-local effects include the effects of the field gradient at the interface. Following Brevet [7] we can write

$$\mathbf{P}^{(2)} = \chi^s \mathbf{E}\mathbf{E} + \gamma \nabla[\mathbf{E}\mathbf{E}] - \nabla[\chi_Q]\mathbf{E}\mathbf{E} \quad (7)$$

Fortunately these terms can be cast into the same form as the surface dipole susceptibility giving effective surface tensor components which are given by

$$\begin{aligned} \chi_{XXZ}^{\text{interface}} &= \chi_{XXZ}^s + \chi_{XXZ}^{\text{eff}} \\ &= \chi_{XXZ}^s + \chi_{ZXZX}^{Q1} \frac{\varepsilon(\omega)}{\varepsilon_1(\omega)} - \chi_{ZXZX}^{Q2} \frac{\varepsilon(\omega)}{\varepsilon_2(\omega)} \end{aligned} \quad (8)$$

$$\begin{aligned} \chi_{XZX}^{\text{interface}} &= \chi_{XZX}^s + \chi_{XZX}^{\text{eff}} \\ &= \chi_{XZX}^s + \chi_{ZXZX}^{Q1} \frac{\varepsilon(\omega)}{\varepsilon_1(\omega)} - \chi_{ZXZX}^{Q2} \frac{\varepsilon(\omega)}{\varepsilon_2(\omega)} \end{aligned} \quad (9)$$

$$\begin{aligned} \chi_{ZXX}^{\text{interface}} &= \chi_{ZXX}^s + \chi_{ZXX}^{\text{eff}} \\ &= \chi_{ZXX}^s + (\gamma_1 + \chi_{ZZXX}^{Q1}) \frac{\varepsilon(\omega)}{\varepsilon_1(\omega)} - (\gamma_2 + \chi_{ZZXX}^{Q2}) \frac{\varepsilon(\omega)}{\varepsilon_2(\omega)} \end{aligned} \quad (10)$$

where the superscript  $s$  specifically indicates the dipole surface terms and  $\text{eff}$  the effective surface contribution of the bulk quadruple and gradient terms.

As pointed out by Brevet and Girault [17], this analysis shows that the discussion of SHG data from liquid/liquid interfaces must be cognisant of the possible contributions from the bulk and from field gradients at the interface. However, in the liquid/liquid case, the changes in optical constants from one bulk phase to the other will normally be less marked than that observed in air/liquid experiments. Of course in the limit of the same optical constants for the two phases, there would be no gradient effects but there would also be no reflection.

In order to extract information on the molecular orientation distribution, the relationship between the macroscopic surface susceptibilities and the molecular hyperpolarizabilities,  $\beta$ , needs to be considered. It is usual to consider the intrinsic non-linear response of each of the molecules as independent of the other molecules so that the interfacial response is an average over the orientational distribution and scales with the molecular density (squared). Even the modification of this response due to local field

effects is usually considered in terms of mean field model and so does not alter the nature of this averaging (three additional diagonal terms need to be included).

$$\chi = \mathbf{T}\{N\langle\beta\rangle\} \quad (11)$$

where  $N$  is the surface number density and  $\langle \rangle$  represents the average over the orientational distribution. The transformation between the molecular axis system ( $ijk$ ) and the interfacial coordinate system ( $IJK$ ) involves the various direction cosines, and the tensors involved are both third rank three rotation matrix terms,  $\mathbf{R}$ , are present [18–20].

$$\chi_{IJK} = N \left\langle \sum_i \sum_j \sum_k R_{li} R_{lj} R_{lk} \beta_{ijk} \right\rangle \quad (12)$$

In many cases it is possible to simplify these equations because only relatively few components of  $\beta$  are significant, either because of the symmetry or the electronic structure of the molecules. When it is possible to reduce the number of distinct significant components to at most two, then it is often possible to extract the ratio of these components and geometric information directly from the observed values of the susceptibility. In these cases the values assumed for the interfacial refractive index and the role of the contributions from the bulk can make a dramatic difference to the derived geometric parameters [21–27].

While some qualitative inferences about the nature of the interface can be derived directly from the SHG observations, extracting detailed quantitative information from the SHG intensity and polarization data requires the construction of a model of the interface and frequently assumptions about some of the parameters for this model. Parameters such as the interfacial refractive index and roughness need to be determined separately, calculated or more frequently obtained by reasonable assumptions [20,21,23–27]. Some idea of the relationship between the model, assumptions and results is given in Figure 1.2.

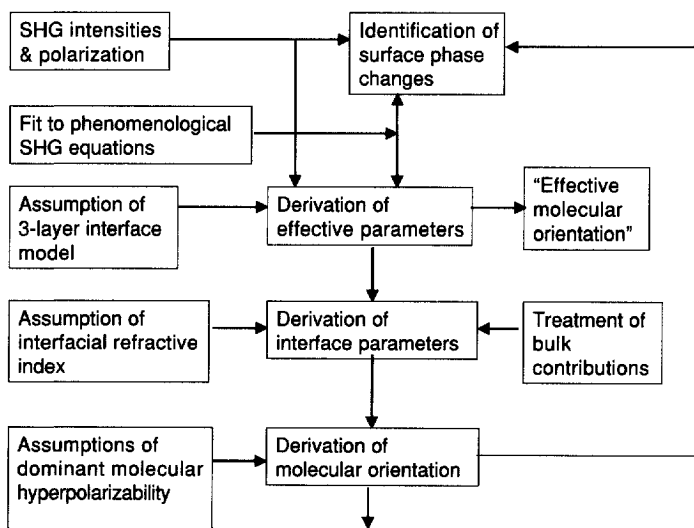


FIGURE 1.2. A guide to the modelling and assumptions needed to interpret the SHG intensity and polarization data.

The SHG results are at their most useful when they can be combined with other measurements and used to validate molecular dynamics simulations of the interface.

### 1.3. EXPERIMENTAL TECHNIQUES

The original surface SHG experiments were frequently performed with low repetition rate ns Nd:YAG lasers at 1064 or 532 nm (Figure 1.3). The low-intensity SHG signals were typically detected with a PMT and Box Car combination and averaged over many laser pulses. Subsequently, SHG spectra were obtained by using a dye laser. Higher repetition rates reduced signal-averaging times. The advantage of the higher intensities available with comparable overall energy (thus no more thermally disruptive of the interface) of ps Ti:Sapphire lasers was soon recognized. These also provide a degree of wavelength scanning. The use of ultra-short (fs) pulses to give a broad wavelength band (or indeed the use of continuum generation to provide an even broader coverage [28]) has enabled SHG spectra on some solid surface to be collected with a CCD detector so that single shot coverage of the whole spectral region is obtained. It is likely that similar techniques will soon be applied to air/liquid and liquid/liquid interfaces.

The interfacial SHG effect is inherently a weak process and there is not the opportunity to build up a phase-matched signal as used, for example, in a doubling crystal. It is therefore frequently necessary or at least useful to use electronically resonant systems to enhance the interfacial SHG signal. This introduces the added complication that  $\chi_{ijk}^{(2)}$  and indeed the interfacial refractive index are complex quantities. Hence, in order to elucidate the real and imaginary components of  $\chi_{ijk}^{(2)}$ , knowledge of the polarization and phase of the surface SHG response is required. A sufficiently extensive set of SHG intensity measurements for a range of different input/output beam polarization combinations can provide the information needed. However, a more elegant approach is to introduce a rotating quarter-wave plate into the experiment to continuously modulate the polarization state of the fundamental beam incident at the interface.

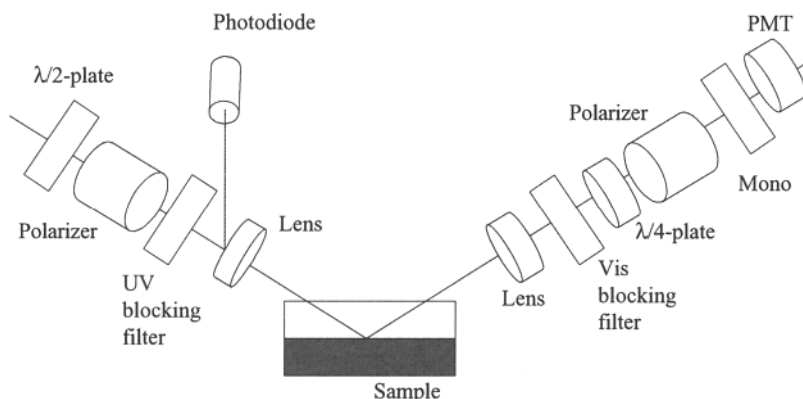


FIGURE 1.3. Diagram of the second harmonic ellipsometry apparatus used to investigate air/liquid and liquid/liquid interfaces.

The alternative is to employ a rotating optical compensator (quarter-wave plate) in the analysis of the SHG radiation generated at the surface to allow the full polarization characteristics of the reflected light to be determined by a Fourier analysis. Such a configuration we use here has been analyzed by Hauge [29,30] applied to the linear-optical ellipsometry case under the title of Generalized Rotating-Compensator Ellipsometry. A rotating compensator has the advantage over the more often employed rotating analyser system in that it enables the unambiguous determination of the polarization state of the light to be determined. An important practical point is that optical compensators usually have low beam deviation. Polarizers, by contrast, very often display beam deviation, and this is particularly true of high-power polarizers, which must be used in these experiments. This leads to the development of the Second Harmonic Ellipsometry technique [31], which will yield more efficient experiments in the future.

From the air/liquid interface, the SHG signal is typically observed in reflection, where the coherent harmonic beam propagates along the same direction as the reflected fundamental beam. The possibility of significant refractive index dispersion in the liquid means that for SHG experiments on the liquid/liquid interface, the harmonic beam path may deviate from the reflected fundamental.

#### 1.4. THE BARE HYDROCARBON/WATER INTERFACE

SHG and SFG have been used to study the neat liquid/liquid interface despite the weak signals observed. At the alkane/water interface a more ordered environment is observed for even chain-length hydrocarbons compared to the odd chain lengths. The ordering is weak and decreases with increasing chain length [32–34]. The dodecane/water interface has been studied along with other hydrocarbon/water interfaces by molecular simulations (hexane/water [35], octane/water [36], nonane/water [37,38], decane/water [39]). From these and low-angle X-ray diffraction experiments, a general picture arises with an interface that is not molecularly sharp [40]. In a typical experimental apparatus the actual interfacial thickness will likely be dominated by the capillary wave motion and this will depend on the interfacial tension [21]. The interfacial tension is usually much less than, for example, the surface tension of water, so some differences can be expected between observations made at the hydrocarbon/water interface compared to the air/water interface. The simulations indicate that there is only a slight degree of interfacial ordering of the hydrocarbon chains, confirming the inferences made from the deviations from Kleinman symmetry observed in SHG experiments. The hydrocarbon chains have a preference for aligning parallel to the interface and there is a weak ordering of the water molecules at the interface in layers, with dipole pointing slightly towards the hydrocarbon and then a higher concentration of water molecules pointing on average away from the interface; it is similar at the water/*n*-alcohol interface [41].

#### 1.5. ADSORPTION OF *PARA*-NITROPHENOL

A number of molecules have become favourites for study at liquid interfaces and there have been a number of investigations of the adsorption behaviour of *p*-nitrophenol

(PNP). PNP molecules exhibit a significant second-order non-linearity and have a UV absorption maximum that is moderately sensitive to the solvent environment though not as dramatic as ET(30) [42,43]. The approximate  $C_{2v}$  symmetry and the planar  $\pi$  electron system suggest that the only significant components of  $\beta$  will be  $\beta_{ZZZ}$ ,  $\beta_{ZXX}$  and  $\beta_{XZX}$ . While this has been conformed by several semi-empirical [44] and ab initio quantum calculations and certainly applies far from resonance, recently some doubt has been cast on these assumptions by DFT calculations [45]. As many of the experiments conducted with PNP exploit the UV resonance to obtain larger signals, care must be exercised with the results of the ab initio calculations as the current codes only evaluate the real part of  $\beta$ .

### 1.5.1. PNP Adsorption at the Hydrocarbon/Water Interface

The adsorption of PNP to a wide variety of interfaces has been studied by SHG. The adsorption isotherm at the dodecane/water interface is shown in Figure 1.4. The adsorption isotherms typically used to fit the surface tension and SHG data at the liquid/liquid interfaces are in terms of the interfacial coverage  $\theta$  and the bulk phase concentration  $c$ , the Langmuir (13) and the Frumkin isotherms (14)

$$\frac{\theta}{1 - \theta} = Kc \quad (13)$$

$$\frac{\theta}{1 - \theta} e^{-2b\theta} = Kc \quad (14)$$

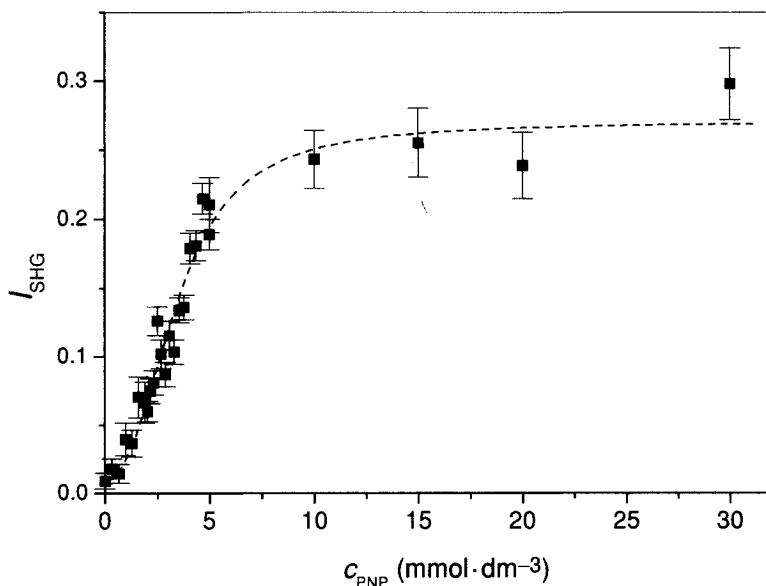


FIGURE 1.4. SHG signal from PNP at the dodecane/water interface. The fit to a Frumkin isotherm is shown as the dotted line. Adapted from ref. [48]; reproduced by permission of the PCCP Owner Societies.

TABLE 1.1. Comparison of the free energy of adsorption for PNP at the air/water and hydrocarbon/water interfaces.

Interface	$-\Delta_{\text{ads}}G^\circ$ (kJ · mol <sup>-1</sup> )	Method
Air/water	16.4 ± 0.2	Surface tension, Frumkin [46]
Hexane/water	17.2 ± 0.3	Surface tension, Frumkin [46]
Heptane/water	25.7	Langmuir [47]
Deodecane/water	25	Langmuir
Deodecane/water	22.0 ± 0.5	Frumkin [48]
Deodecane/water	20.0 ± 0.5	Frumkin and order terms [48]

where  $K$  is the adsorption equilibrium constant and  $b$  an interaction parameter that describes the interactions between adsorbate molecules. The isotherms are shown here in terms of the concentration of the adsorbate  $c$  in one of the liquid phases. If the isotherm is defined in terms of the mole fraction of the adsorbate in this phase then the equilibrium constants and associated free energies are related by a scaling factor (the molarity of the solvent; see Appendix).

Considerable care needs to be taken in extracting the interfacial concentration from the SHG intensities because of the interaction between surface density and surface order on the SHG process [49]. Table 1 shows a comparison of the values of  $\Delta_{\text{ads}}G^\circ$  for PNP at the air/water and hydrocarbon/water interfaces determined by SHG methods. The different results obtained at the dodecane/water interface where different isotherms were used to fit the SHG data suggest that the determination of  $-\Delta_{\text{ads}}G^\circ$  at the heptane/water interface using only a Langmuir isotherm gives a value that is too high and thus this value should be re-examined.

### 1.5.2. PNP Adsorption in the Presence of Tributyl Phosphate

The addition of tributyl phosphate (TBP) to the dodecane acts to reduce the SHG signal from an initial (partial) monolayer of PNP at the dodecane/water interface; the dependence shown in Figure 1.5 can be fitted to a Langmuir-like equation (15) from which an effective free energy of adsorption for TBP,  $\Delta_{\text{ads}}G_{\text{TBP}}^\circ$ , can be extracted [48].

$$I_{\text{SHG}} = I_0 \left( 1 - \frac{kc}{1 + kc} \right)^2 \quad (15)$$

The value of  $\Delta_{\text{ads}}G_{\text{TBP}}^\circ$  determined in this manner is linearly dependent on the concentration of PNP. Extrapolating to zero PNP concentration gives  $\Delta_{\text{ads}}G_{\text{TBP}}^\circ = -31.4 \pm 0.8 \text{ kJ} \cdot \text{mol}^{-1}$ , which is consistent with the value determined by surface pressure and surface tension measurements at low TBP concentrations [50,51] (when corrected for the different interface standard states, see Appendix).

The possibility of absorption of the SHG signal by the upper medium complicates the interpretation of SHG from liquid/liquid studies compared to similar studies of the air/liquid interface. The same problem is of course faced by studies of the liquid/solid interface or total internal reflection studies at the air/liquid interface. In the case of the experiments on the dodecane/water interface, the possibility existed that the absorption

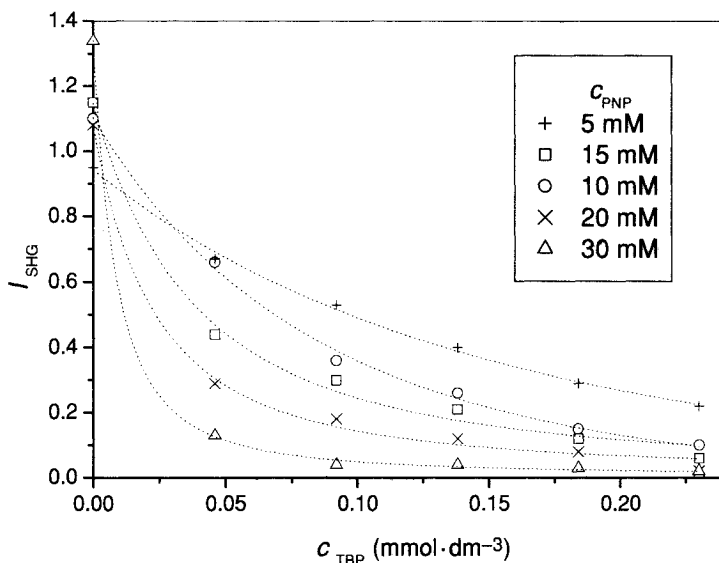


FIGURE 1.5. The SHG signal from PNP at the dodecane/water interface is reduced on addition of TBP to the dodecane. Adapted from ref. [48]; reprinted by permission of the PCCP Owner Societies.

of the harmonic wavelength (282 nm) by the TBP ( $\lambda_{\max} = 220$  nm) could account for the decrease in the observed SHG intensity as a function of increasing concentration of TBP. However, this decrease was observed for addition of TBP to an interface loaded with a high concentration of PNP, but an increase in SHG signal was observed when TBP was added at low PNP concentrations. It was thus possible to conclude that absorption by TBP was not the cause of the reduction in SHG intensity. Nonetheless, it is likely that some SHG intensity was lost by absorption by the dodecane solvent and the experiment's sensitivity could be improved by using a thinner layer of overlying solvent.

## 1.6. FLOW CELL EXPERIMENTS

The static experiments show that there is a complex between TBP and PNP at the dodecane/water interface. Even by simply mixing the two solutions it was clear that this interaction was time-dependent. However, the decay rate was sufficiently fast so that given the need to ensure uniform mixing in the bulk phases and the time required to accumulate a reasonable S/N, only the long time tail of the decay curve could be measured. No accurate estimate of the decay rate could be made in the Petri-dish. The solution was to construct a flow cell to measure the kinetics of the TBP and PNP interaction at the dodecane/water interface [48].

The design of the flow cell (Figure 1.6) ensured that a stable dodecane/water interface would form and then allow the two liquids to be separated. The flow rate was variable and the interface could be probed at various distances along the flow. The cell contained two horizontal flat glass plates located on the central plane of the cell that

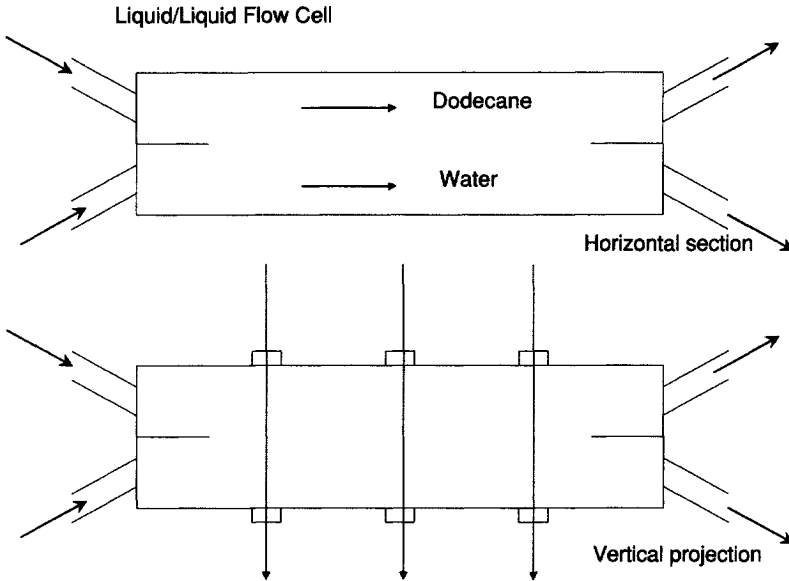


FIGURE 1.6. Liquid/liquid flow cell.

stabilize the incoming fluid flows and allow a stable interface to form. Initially the flow was driven by two peristaltic pumps each pumping one fluid from a main reservoir to the flow cell, from which a drain returned the fluid back to the main reservoir. The flow rates of the two fluids could be controlled independently to form an interface that was stable over a period of up to an hour. However, the peristaltic pumps produced ripples on the interface that were avoided by using gravity feed systems with the pumps used to refill small reservoirs; overflows in each reservoir ensured a constant pressure head.

$\text{CaF}_2$  windows along the cell were used as silica windows that developed significant SHG signals with exposure to the high laser beam energies. However, the tight focusing used for this experiment led to damage to the windows after prolonged use and were replaced as required. The thickness of the dodecane layer meant that higher laser intensities were required to achieve a good S/N ratio, than were needed for the static experiments.

The flow cell "translates" time into distance and the combination of the three and varying the flow rates gave a range of observations from 0 to 30 s. SHG measurements of the static aqueous/dodecane interface were made at each port before and after the flow experiment to calibrate the observations from each port. For a laminar (non-turbulent) flow, the two flow rates should be in the inverse ratio of the fluid viscosities; this ratio for dodecane on water is 0.65 at 25°C, very close to the observed flow rate ratio of 0.67. The bulk flow rates for each liquid were measured by collecting the volume of liquid flowing in a known time. Since the cell operates under non-turbulent conditions, the velocity of each layer at the interface must be the same, but the average velocities of the two layers are different. Ideally a model of the flow conditions inside the cell would be used to accurately determine the velocity of the interface. Since this was not

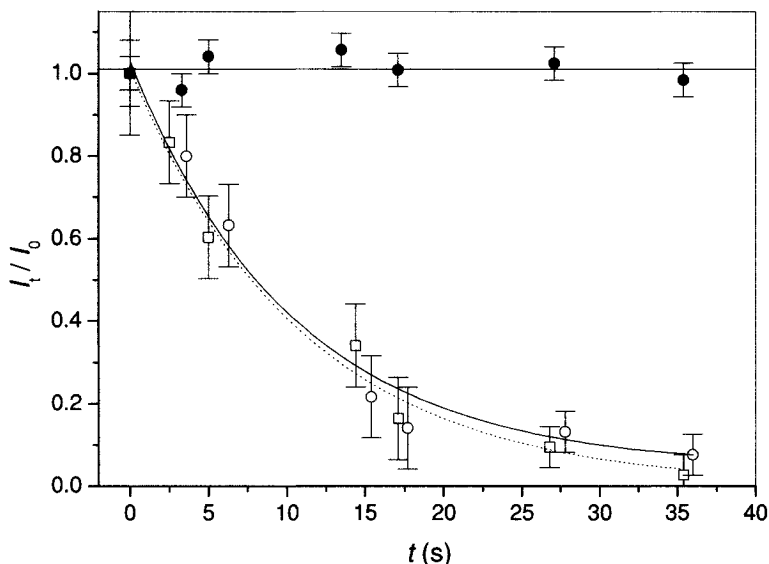


FIGURE 1.7. The decay of the SHG signal from PNP at the dodecane/water interface as a function of time from the formation of the interface. The full circles are the signals in the absence of TBP and the open circles and squares are two experiments in the presence of TBP. Adapted from ref. [48]; reproduced by permission of the PCCP Owner Societies.

available and since the flow rates used are very low, it is reasonable to make a first approximation that the velocity of the interface will be the average velocities of the two layers. The rapid equilibration of PNP at the newly formed dodecane/water interface is demonstrated in Figure 1.7. The PNP SHG signal, corrected for the water/dodecane background and the variation due to the windows, is constant over the time periods used for the later experiments. This is consistent with the rapid equilibration of the PNP signal at the air/water interface measured using a liquid jet. The SHG signals for the PNP/TBP system, similarly corrected and normalized to the signal at time zero are shown in Figure 1.7. As expected from the static experiments, for the concentrations of PNP and TBP used, the SHG signal decays monotonically to the background level. Assuming the intensity is proportional to the square of the surface coverage, the rate constant for reordering at the surface [48] is  $k = 0.5 \pm 0.05 \text{ s}^{-1}$ .

For comparison, the measured adsorption rate for PNP to the air/water interface gave a rate constant of  $k = 4.4 \pm 0.2 \times 10^4 \text{ s}^{-1}$  but a desorption rate of  $6 \pm 2 \text{ s}^{-1}$  [52]. The rapid adsorption to the air/water interface is quite consistent with the very rapid establishment of the SHG signal from PNP at the dodecane/water interface observed in these flow cell experiments. However, the observed decay rate constant in the presence of TBP of ca.  $0.5 \text{ s}^{-1}$  is much faster than the desorption rate constant that would be implied from the air/water experiments. This further implicates a reorganization process involving bonding between TBP and PNP as the cause of the loss of SHG intensity, which results in an overall loss of orientational order.

The addition of TBP in the dodecane increases the free energy of adsorption of PNP in a manner consistent with the formation of an interfacial complex between TBP and

PNP. We suggest that with the TBP present on the dodecane side of the interface, the preferential orientation of the TBP PNP complex will be opposite to that for uncomplexed PNP. For a mixture of complexed and uncomplexed PNP this will result in an overall reduction in the overall net orientation, that is, a reduction in the orientational order and a consequent reduction in the SHG intensity. This situation provides an explanation for a reduction in SHG intensity even when there is an increasing surface concentration of the PNP.

### 1.7. DYE MOLECULES AT THE DODECANE/WATER INTERFACE

Dye molecules have been popular adsorbates for optical studies at interfaces because of their accessible electronic resonances and the consequent large absorption and, most usefully, large fluorescence cross sections that enable even single molecule studies. Linear optical techniques have limitations when the molecules are present in the adjacent bulk phases as it is difficult to distinguish the interfacial species from the more prevalent bulk. SHG has proved useful in studying monolayers of dye molecules at the air/solid interface [53–60] and Langmuir–Blodgett films [61–66], situations in which the molecules are only present at the interfacial layer. The complications in interpretation of the non-linear technique compared to linear ellipsometric experiments become most worthwhile when the dye molecules at interface are in equilibrium with the bulk solvent. There have been a number of such studies at the air/water [67,68] and air/hydrocarbon interfaces, but relatively fewer at the corresponding liquid/liquid interface [69]. Some of the most popular dyes used in SHG studies are the rhodamine series, malachite green [70,71], oxazines [72] and eosin B [73,74]. The interactions between the dye molecules, their tendency to form dimers, clusters and large aggregates in a manner that depends on the environment also make these species ideal for probing the chemical physics of the interfacial region. Many studies have suggested that dimer species predominate at the air/solvent interface even at relatively low solution concentrations.

The adsorption isotherm of rhodamine 6G at the dodecane/water interface was recorded by SHG [75] at 564 nm and using the phase difference between the bare interface and the dye harmonic fields derived from the very low concentration limit of the isotherm, the second-order susceptibility from the dye can be derived from the SHG intensity, and the resulting data set is shown in Figure 1.8 together with a fit to a Frumkin isotherm at low concentrations and a separate Langmuir phase at higher concentrations. The phase transition is seen more clearly in the reciprocal plot where in addition the polarization changes ( $A$  and  $B$  from Equation 5) are also seen to occur at the same bulk dye concentration (ca. 6  $\mu\text{M}$ ). The coefficients obtained by least-squares fitting to both the Langmuir and Frumkin isotherms are summarized in Table 2.

The formation of dimers in solution at higher concentrations indicates an interaction between the dye molecules and so the  $b$  term in the Frumkin isotherm is not a surprise. The adsorption behaviour suggests that the dye is highly surface-active and formation of a monolayer is almost complete by the transition at ca. 6  $\mu\text{M}$ . The standard free energy of adsorption derived from the isotherm is consistent with a monolayer coverage forming even at the micromolar aqueous concentrations. Once the first layer is substantially complete, subsequent adsorption takes place on this layer to form a second-ordered layer,

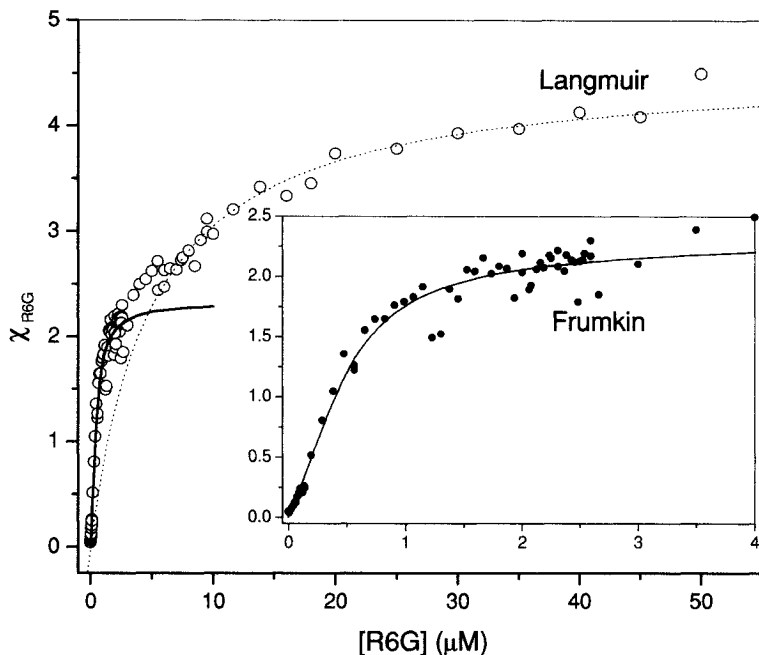


FIGURE 1.8. The “Frumkin” isotherm (full line) is a high quality fit to the low concentration region with a transition (see Figure 1.5) to a “Langmuir” isotherm (dotted line) for the higher concentration region.

though the polarization data suggests that the nature of the order in the “second” layer is different. The free energy of adsorption is lower for the second layer, but still substantial. The formation of second- and multiple-ordered dye layers has been previously observed at the air/solid interface [56] and air/liquid interface.

Extrapolating each isotherm to infinite concentration, gives the susceptibility of the full monolayer (which is the value of  $S$  on an arbitrary scale). The ratio  $S_{\text{Lang}}/S_{\text{Frum}} \cong 2$  is very suggestive of a packing of the dye molecules that is twice as dense in the phase in equilibrium with the bulk above a concentration of 6  $\mu\text{M}$ . This suggests that in keeping with previous observations of dimer formation at the interface, an alternative way to view such a pair of ordered layers may be as adsorbed dimers.

TABLE 1.2. The coefficients obtained by fitting the Frumkin below the 6- $\mu\text{M}$  transition and Langmuir isotherms above the transition.

	Frumkin	Langmuir
$S$	2.34	4.57
$K$	$0.993 \times 10^6$	$0.2 \times 10^6$
$B$	-1.48	
$\Delta G^\circ$ ( $\text{kJ} \cdot \text{mol}^{-1}$ )	-33.3	-29.4

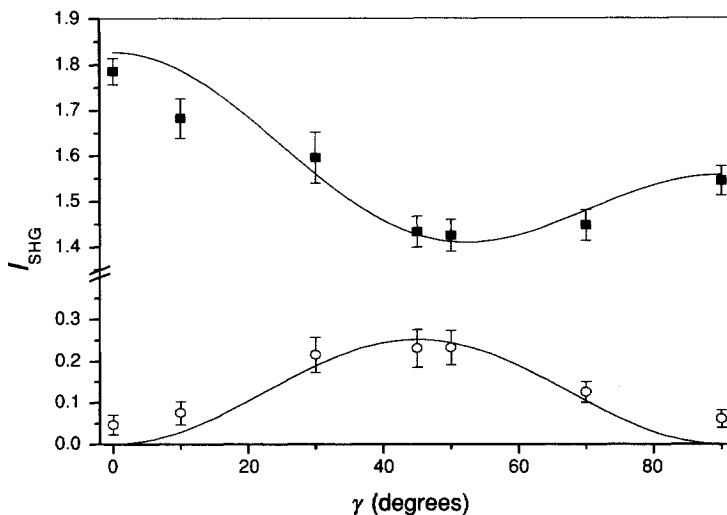


FIGURE 1.9. The dependence of the S- (circles) and P- (squares) polarized second harmonic as a function of the polarization of the fundamental for a dye concentration of  $10 \mu\text{M}$  in the aqueous phase.

The polarization curves for concentrations higher than  $6 \mu\text{M}$  can be fit by Equations (5) and (6) and Figure 1.9 shows the S- and P-polarized harmonic data for the  $10\text{-}\mu\text{M}$  solution. Similar results have been reported for SHG experiments on the rhodamine dyes at various interfaces. The best fit is obtained by introducing a phase difference,  $\eta$ , between the parameters  $A$  and  $B$  consistent with the complex nature of the susceptibilities on resonance. A plot of the concentration dependence of the  $A/B$ , given in Figure 1.10, shows that a relatively sharp transition takes place in the structure of the interface at an aqueous dye concentration of ca.  $6 \mu\text{M}$ .

The clear transition in the polarization behaviour that occurs at about  $6 \mu\text{M}$  shows that the structure of the interface has changed. It is likely that this corresponds to reaching a critical packing density at which a change of phase takes place and the adsorbed layer corresponds to a collection of dye dimers at the interface. The formation of multiple layers has been observed with spin-coated films although multilayers of Rhodamine B have been deposited from solution without a change being observed in the layer structure. Similarly the predominance of dimers at interfaces has been inferred previously but in the current situation we are able to observe the transition between monomers and dimers at the interface.

## 1.8. ELECTROCHEMICAL LIQUID/LIQUID INTERFACES

While there have been many SHG studies at the solid electrode/liquid interface as both an in situ probe of the electrode interface and the influence of adsorption at the surface of the electrode, there have been far fewer studies of electrochemical processes occurring at the boundary between two immiscible electrolyte solutions.

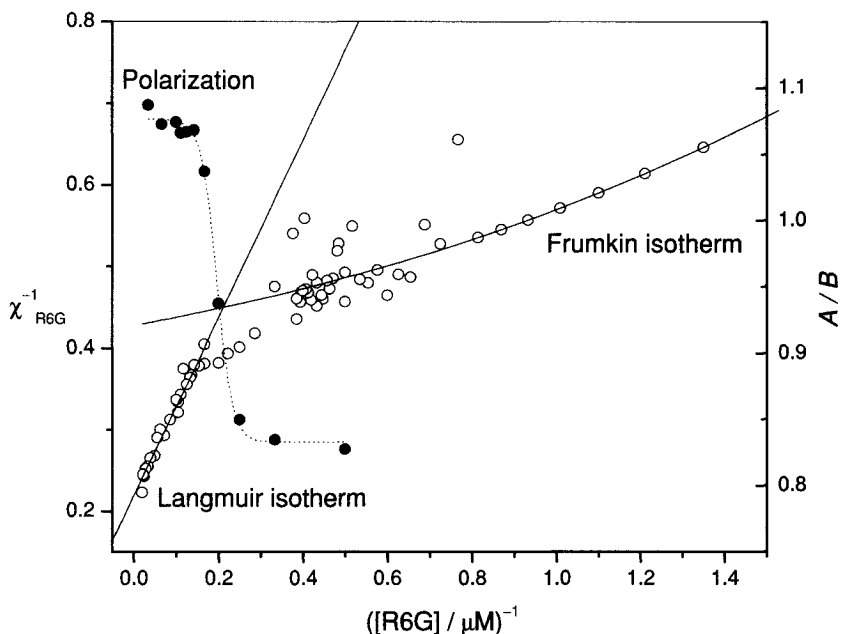


FIGURE 1.10. Plot of the reciprocal of the dye susceptibility vs. the reciprocal of the dye concentration in the aqueous phase. A relatively sharp transition is seen at around  $6 \mu\text{M}$  and a similar transition is seen in the ratio  $A/B$  (see Equation 5) derived from the polarization curves.

Higgins and Corn [76,77] have studied the response of an adsorbed layer of 2-(*N*-octadecyl)aminonaphthalene-6-sulfonate at the water/1,2-dichloroethane interface as a function of applied potential and showed how the ordering at the interface is influenced by the applied potential.

We have studied the interactions of the crown ether 4-nitrobenzo-15-crown-5 at the water/dichloroethane interface [78] (Figure 1.11). The variation of the SHG signal from this crown ether as a function of potential across the interface depends dramatically on the presence or absence of sodium ions. The neutral crown ether behaves quite differently from the charged cation-crown ether complex. At the heptane/water interface, cation binding has been studied using dye-labelled crowns [79]. We are currently investigating the behaviour of other crown ethers at the air/water and solvent/water interfaces.

“Solid” models for these liquid/liquid interfaces in which one of the solutions is replaced by a polymer, often swollen with a significant proportion of solvent, have proved useful in SHG studies of analytically relevant studies of liquid/liquid junctions, for example, the study of crown ether ionophores imbedded in a PVC film.

## 1.9. CHIRAL MOLECULES AT LIQUID/LIQUID INTERFACES

The SHG provides a very useful method to study chiral molecules. The lack of inversion symmetry at the interface means that electric dipole terms can contribute to effects that have similar (but not identical) consequences to conventional optical activity.

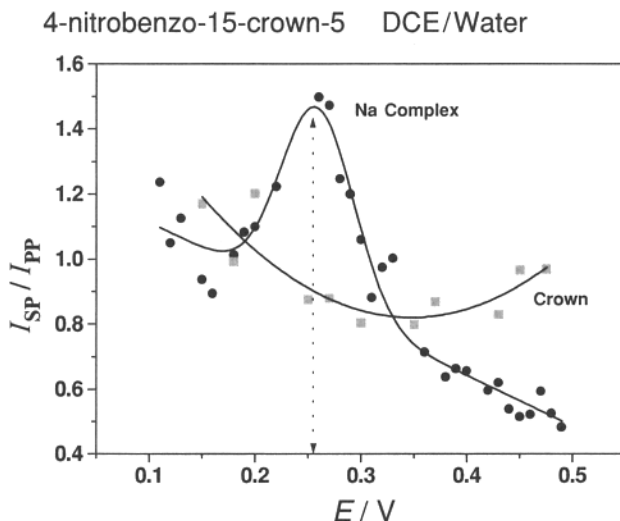


FIGURE 1.11. The variation of the crown ether SHG signal as a function of the applied potential across the dichloroethane/water interface.

The presence of the  $\chi_{XYZ}$  term gives rise to a circular differential scattering (SHG-CD) and to an optical rotation (SHG-ORD) of the harmonic beam. For example, in the absence of this term, a p-polarized fundamental gives rise to a p-polarized harmonic, but in its presence the harmonic field is rotated; the rotation angle is wavelength-dependent and is opposite in sign for the two enantiomers. A number of systems have been studied at the solid and air/water interfaces and the experiments are now being extended to the liquid/liquid interface. Figure 1.12 shows a comparison of the SHG-ORD for the dipeptide Boc-Trp-Trp at the air/water and heptane/water interfaces.

### 1.10. SHG FROM MICELLES AND LIPOSOMES

SHG has more recently been shown to be a viable technique for the observation of even symmetrical (e.g. spherical) microparticle surfaces. Locally, the regions of the microparticle surface are non-centrosymmetric (inside vs. outside) and thus can generate the harmonic field. For large particles the field generated from sections of the interface on opposite sides of the particle would cancel as these interfaces point in opposite directions, that is, overall there is a centre of inversion. However, if the particle is comparable in size to the wavelength of the (incident) light, then the fields generated from opposite sides of the particle can add constructively. Taking an extreme view, for a particle of size  $\lambda$ , the phase of the fundamental field will be  $180^\circ$  different for the two interfaces of the microparticle, and thus the phase inversion of the radiation exactly counters the inversion of the molecules because of the opposite orientation of the interface [80–82].

Using this idea it has been possible to study the interfaces of polystyrene beads in aqueous suspensions [83], semiconductor and clay particles [84]; more relevant to